Enhancing the absorption coefficient of a backed rigid frame porous layer by embedding circular periodic inclusions

J.-P. Groby,[a] O. Dazel, and A. Duclos
Laboratoire d'Acoustique de l'Université du Maine, UMR6613 CNRS/Université du Maine, Avenue Olivier Messiaen, F-72085 Le Mans Cedex 9, France

L. Boeckx
Huntsman Europe, Everslaan 45, B-3078 Everberg, Belgium

L. Kelders
Laboratory of Acoustic and Thermal Physics, KULeuven, Celestijnenlaan 200-D, B-3001 Heverlee, Belgium

(Received 30 November 2010; revised 31 August 2011; accepted 18 September 2011)

The acoustic properties of a porous sheet of medium static air flow resistivity (around 10 000 $\mathrm{N\,m\,s^{-4}}$), in which a periodic set of circular inclusions is embedded and which is backed by a rigid plate, are investigated. The inclusions and porous skeleton are assumed motionless. Such a structure behaves like a multi-component diffraction grating. Numerical results show that this structure presents a quasi-total (close to unity) absorption peak below the quarter-wavelength resonance of the porous sheet in absence of inclusions. This result is explained by the excitation of a complex trapped mode. When more than one inclusion per spatial period is considered, additional quasi-total absorption peaks are observed. The numerical results, as calculated with the help of the mode-matching method described in this paper, agree with those calculated using a finite element method.
 [DOI: 10.1121/1.3652865]

PACS number(s): 43.55.Ev, 43.20.Fn, 43.20.Ks, 43.20.Gp [KVH] Pages: 3771–3780

I. INTRODUCTION

Porous materials suffer from a lack of absorption at low frequencies, when compared to their efficiency at higher frequencies. The purpose of the present article is to investigate an alternative to multi-layering by considering periodic inclusions embedded in a porous sheet attached to a rigid plate. This configuration results in a diffraction grating and a sonic- crystal,[1] constituted by the grating and its image or by the combination of grating, used in reflection. The inclusions and porous skeleton are assumed motionless.

The influence of a volume heterogeneity on absorption and transmission of a porous layer without rigid backing was previously investigated by use of the multipole method in Refs. 1 and 2. This was done by embedding a periodic set of high-contrast inclusions in a macroscopically homogeneous porous layer. The sizes of the inclusions are comparable to the wavelength in the porous medium, and the thickness and weight of the porous layer are relatively small for better efficiency when compared to those of usual multilayered packages. This leads either to an increase of the absorption coefficient, in the case of one layer of inclusions, or to band-gaps and a total absorption peak, in case of multi-layered set of inclusions (sonic crystal). The influence on the absorption was explained by mode excitation of the configuration, enabled by the periodic inclusions, whose structure leads to energy entrapment. Other works related to volume heterogeneities in macroscopically homogeneous porous material were carried out essentially by means of the homogenization procedure,[3,4] possibly leading to double porosity materials,[5] when the wavelength is larger than the size of heterogeneities.

The influence of the irregularities of the rigid plate, on which porous sheets are often attached, on the absorption coefficient was previously investigated by use of the multimodal method in Ref. 6, by considering periodic rectangular irregularities filled with air. In the particular case of one irregularity per spatial period, this leads to a total absorption peak associated with excitation of the fundamental modified mode of the backed plate. This is excited thanks to the surface grating. Other works related to surface irregularities were carried out, notably related to local resonances associated with fractal irregularities.[7,8]

Local resonance and trapped modes are another possibility to localize the field. Trapped modes were largely studied in waveguides[9] or in periodic structures.[10] Here, both theoretically and numerically, we investigate the changes in the absorption coefficient due to the embedding of a multiple inclusions grating in a rigid frame porous layer glued against a rigid wall. The effects of the modified mode of the plate and Bragg interference are clearly visible on the absorption curve, while a quasi-total (close to unity) absorption is obtained for a frequency below the fundamental quarter-wavelength resonance of the backed porous sheet. This peak exhibits some of the specific features of a trapped mode excitation.

II. FORMULATION OF THE PROBLEM

A. Description of the configuration

Both the incident plane acoustic wave and the porous layer are assumed to be invariant with respect to the

[a]Author to whom correspondence should be addressed. Electronic mail: Jean-Philippe.Groby@univ-lemans.fr

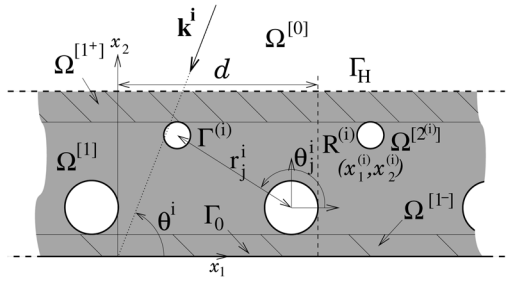

FIG. 1. Cross-sectional plane view of the configuration.

Cartesian coordinate x_3. A cross-sectional $x_1 - x_2$ plane view of the 2D scattering problem is shown Fig. 1.

Before the addition of the cylindric inclusions, the layer is made of a porous material saturated by air (e.g., a foam), which is modeled (by homogenization) as a macroscopically homogeneous equivalent fluid $M^{[1]}$. The porous sheet is backed by a rigid surface. The upper and lower flat, mutually-parallel boundaries of the layer, whose x_2 coordinates are H and 0, are designated by Γ_H and Γ_0, respectively. $M^{[0]}$, the ambient fluid that occupies $\Omega^{[0]}$, and $M^{[1]}$ are in firm contact through Γ_H, making the pressure and normal velocity continuous across Γ_H ($[p(\mathbf{x})] = 0$ and $[\rho^{-1}\partial_n p(\mathbf{x})] = 0$, wherein $\mathbf{n}$ denotes the generic unit vector normal to a boundary and ∂_n designates the operator $\partial_n = \mathbf{n} \cdot \nabla$). Γ_0 is rigid [Neumann type boundary conditions, $\partial_n p(\mathbf{x}) = 0$].

N^c inclusions, with a common spatial periodicity d, are embedded in the porous layer and create a diffraction grating in the x_1 direction. Depending on the arrangement of the N^c inclusions in the unit cell, a diffraction grating or a sonic-crystal of period d^c can be formed ($d^c \leq d$). The set of indices by which the cylinders within the unit cell are identified is denoted by $\mathcal{N}^c \in \mathbb{N}$. The jth inclusion occupies the disk $\Omega^{[2^{(j)}]}$ of radius $R^{(j)}$ and is centered at $\mathbf{x}^{(j)} = (x_1^{(j)}, x_2^{(j)})$, $j \in \mathcal{N}^c$. The inclusions are infinitely rigid (Neumann type boundary conditions on $\Gamma^{(j)}$), i.e., the contrast between the material that occupies $\Omega^{[2^{(j)}]}$ and $M^{[1]}$ is very large. This also means that the inclusions can consist in rigid tubes or holes posteriorly processed to create a rigid bound, because the only important thing is the Neumann type boundary conditions at the exterior boundary of the inclusion. This process can be used to reduce the weight of the final structure. Two subspaces $\Omega^{[1^{\pm}]} \in \Omega^{[1]}$ are also defined, corresponding to the upper and lower part, respectively, of the porous layer without inclusions. The inclusions and porous skeleton are assumed motionless.

The total pressure, wavenumber, and wave speed are denoted by the generic symbols p, k, and c, respectively, with $p = p^{[0]}, k = k^{[0]} = \omega/c^{[0]}$ in $\Omega^{[0]}$, and $p = p^{[1]}, k = k^{[1]} = \omega/c^{[1]}$ in $\Omega^{[1]}$, wherein $\omega = 2\pi\nu$ is the angular frequency, with ν the frequency.

Rather than to solve directly for the pressure $\bar{p}(\mathbf{x}, t)$ [with $\mathbf{x} = (x_1, x_2)$], we prefer to deal with $p(\mathbf{x}, \omega)$, related to $\bar{p}(\mathbf{x}, t)$ by the Fourier transform $p(\mathbf{x}, \omega) = \int_{-\infty}^{\infty} \bar{p}(\mathbf{x}, t) e^{i\omega t} dt$. Henceforth, we drop the ω in $p(\mathbf{x}, \omega)$ so as to denote the latter by $p(\mathbf{x})$.

The wavevector $\mathbf{k}^i$ of the incident plane wave lies in the sagittal plane and the angle of incidence is θ^i measured counterclockwise from the positive x_1 axis. The incident wave propagates initially in $\Omega^{[0]}$ and is expressed by $p^i(\mathbf{x}) = A^i e^{i(k_1^i x_1 - k_2^{[0]i}(x_2 - H))}$, wherein $k_1^i = -k^{[0]} \cos\theta^i$, $k_2^{[0]i} = k^{[0]} \sin\theta^i$, and $A^i = A^i(\omega)$ is the signal spectrum.

The plane wave nature of the incident wave and the periodic nature of $\bigcup_{j \in \mathcal{N}^c} \Omega^{[2^{(j)}]}$ imply the Floquet relation

$$p(x_1 + qd, x_2) = p(x_1, x_2) e^{ik_1^i qd}; \forall \mathbf{x} \in \mathbb{R}^2; \forall q \in \mathbb{Z}. \quad (1)$$

Consequently, it suffices to examine the field in the central cell of the plate.

The uniqueness of the solution to the forward-scattering problem is ensured by the radiation condition:

$$p^{[0]}(\mathbf{x}) - p^i(\mathbf{x}) \sim e^{i\mathbf{k}^{[0]} \cdot \mathbf{x}} / \sqrt{|\mathbf{x}|}, \quad |\mathbf{x}| \to \infty, \quad x_2 > H. \quad (2)$$

B. Material modeling

Rigid frame porous material M is modeled using the Johnson-Champoux-Allard model. The dynamic compressibilty K and dynamic density ρ, linked to the sound speed through $c = \sqrt{1/(K\rho)}$ are[11,12]

$$\frac{1}{K} = \frac{\gamma P_0}{\phi\left(\gamma - (\gamma - 1)\left(1 + i\frac{\omega_c'}{\mathrm{Pr}\omega} G(\mathrm{Pr}\omega)\right)^{-1}\right)},$$
$$\rho = \frac{\rho_f \alpha_\infty}{\phi}\left(1 + i\frac{\omega_c}{\omega} F(\omega)\right), \quad (3)$$

wherein $\omega_c = \sigma\phi/\rho_f\alpha_\infty$ is the Biot frequency, $\omega_c' = \sigma'\phi/\rho_f\alpha_\infty$, γ the specific heat ratio, P_0 the atmospheric pressure, Pr the Prandtl number, ρ_f the density of the fluid in the (interconnected) pores, ϕ the open porosity, α_∞ the high frequency limit of the tortuosity, σ the static air flow resistivity, and σ' the static thermal resistivity. The scaling functions $G(\mathrm{Pr}\omega)$[13] and $F(\omega)$[14] are given by

$$G(\mathrm{Pr}\omega) = \sqrt{1 - i\eta\rho_f \mathrm{Pr}\omega\left(\frac{2\alpha_\infty}{\sigma'\phi\Lambda'}\right)^2},$$
$$F(\omega) = \sqrt{1 - i\eta\rho_f\omega\left(\frac{2\alpha_\infty}{\sigma\phi\Lambda}\right)^2}, \quad (4)$$

where η is the dynamic viscosity of the fluid, Λ' the thermal characteristic length, and Λ the viscous characteristic length. The "static thermal resistivity" is related to the thermal characteristic length through $\sigma' = 8\alpha_\infty\eta/\phi\Lambda'^2$ (Ref. 13).

While the configuration is similar to those already studied in Refs. 1 and 2, it is different in that the porous sheet is backed by a rigid plate, but also more complex in that the unit cell can be composed of more than one non overlapping inclusion, when the x_2-coordinates of the center of two inclusions are separated by a distance lower than the sum of their radii. In this latter case, the interaction between these inclusions cannot be modeled as exposed in Ref. 1, and a more complex interaction model should be employed.[15] The method of solution is also briefly summarized hereafter.

C. Field representations in $\Omega^{[0]}$ and $\Omega^{[1^{\pm}]}$

The continuity relations across the interfaces Γ_H and Γ_0 are first considered in Sec. III A. The field representations in $\Omega^{[0]}$ and $\Omega^{[1^{\pm}]}$ are needed as the first step. The continuity conditions across $\Gamma^{(j)}$, $\forall j \in \mathcal{N}^c$ will be treated in Sec. III B.

Separation of variables, the radiation condition, and the Floquet theorem lead to the representation

$$p^{[0]}(x) = \sum_{q\in\mathbb{Z}} \left[e^{-\mathrm{i}k_{2q}^{[0]}(x_2-H)}\delta_q + R_q e^{\mathrm{i}k_{2q}^{[0]}(x_2-H)} \right] e^{\mathrm{i}k_{1q}x_1}, \quad \forall \mathbf{x} \in \Omega^{[0]}, \tag{5}$$

wherein δ_q is the Kronecker symbol, $k_{1q} = k_1^i + 2q\pi/d$, $k_{2q}^{[0]} = \sqrt{(k^{[0]})^2 - (k_{1q})^2}$ with $\mathrm{Re}\left(k_{2q}^{[0]}\right) \geq 0$ and $\mathrm{Im}\left(k_{2q}^{[0]}\right) \geq 0$. R_q is the reflection coefficient of the plane wave denoted by the subscript q.

It is first convenient to use Cartesian coordinates (x_1, x_2) to represent the field in $\Omega^{[1^{\pm}]}$. This field is composed of the diffracted field in the plate and the fields scattered by the inclusions, whose form depends on the position of **x,** either below or above the inclusions.[16] Refering to Ref. 1, whatever the arrangement of the inclusions, x_2 is always larger than $\max_{j\in\mathcal{N}^c}\left(x_2^{(j)} + R^{(j)}\right)$ in $\Omega^{[1^+]}$, while x_2 is always smaller than $\min_{j\in\mathcal{N}^c}\left(x_2^{(j)} - R^{(j)}\right)$ in $\Omega^{[1^-]}$. The total field in $\Omega^{[1^{\pm}]}$ can be written in Cartesian coordinates as

$$\begin{aligned} p^{[1^{\pm}]}(\mathrm{x}) = &\sum_{q\in\mathbb{Z}} \left(f_q e^{-\mathrm{i}k_{2q}^{[1]}x_2} + g_q e^{\mathrm{i}k_{2q}^{[1]}x_2} \right) e^{\mathrm{i}k_{1q}x_1} \\ &+ \sum_{q\in\mathbb{Z}} \sum_{j\in\mathcal{N}^c} \sum_{l\in\mathbb{Z}} K_{ql}^{\pm} B_l^{(j)} e^{\mathrm{i}\left(k_{1q}\left(x_1 - x_1^{(j)}\right)\right) \pm k_{2q}^{[1]}\left(x_2 - x_2^{(j)}\right)}, \end{aligned} \tag{6}$$

wherein $B_l^{(j)}$ are the coefficients of the field scattered by the jth cylinder of the unit cell, f_q and g_q are the coefficients of the diffracted waves inside the layer associated with the plane wave denoted by q, and $K_{ql}^{\pm} = 2(-\mathrm{i})^l e^{\pm \mathrm{i}l\theta_q}/dk_{2q}^{[1]}$ with θ_q such that $k^{[1]}e^{\mathrm{i}\theta_q} = k_{1q} + \mathrm{i}k_{2q}^{[1]}$ (Ref. 15).

III. DETERMINATION OF THE ACOUSTIC PROPERTIES OF THE CONFIGURATION

A. Application of the continuity conditions across Γ_H and Γ_0

The continuity of the pressure field and of the normal component of the velocity is applied across Γ_H and the Neumann condition is applied on Γ_0. After introducing the proper field representations therein, i.e., Eqs. (5) and (6), and making use of the orthogonality relation $\int_{-d/2}^{d/2} e^{\mathrm{i}(k_{1n}-k_{1l})x_1}\mathrm{d}x_1 = d\delta_{nl}$, $\forall (l,n) \in \mathbb{Z}^2$, a linear set of equations results. After some algebra and rearrangements, this linear set reduces to a coupled system of equations for solution of R_q, f_q and g_q in terms of $B_l^{(j)}$.

B. Application of the multipole method

The expressions of f_q and g_q in terms of $B_l^{(j)}$ are introduced in the so-called diffracted field inside the layer. The latter field accounts for the direct, diffracted waves inside the layer and for the reflected waves at the boundaries Γ_0 and Γ_H, previously scattered by each inclusions. This expression, when compared with the expression of the direct scattered field by the inclusions, is valid in the whole domain $\Omega^{[1]}$. To proceed further, the Cartesian form of this field is converted to the cylindrical harmonic form in the polar coordinate system attached to each inclusion, as stated for example in Ref. 1. Effectively, central to the multipole method are the local field expansions or multipole expansions around each inclusion.

Introducing $A_L^{(J)}$, the coefficient of the locally-incident field, the pressure field in the vicinity of the Jth inclusion, in terms of its attached coordinate system, reads as

$$\begin{aligned} p^{[1]}(\mathrm{r}_J) = &\sum_{L\in\mathbb{Z}} B_L^{(J)} H_L^{(1)}\left(k^{[1]}r_J\right) e^{\mathrm{i}L\theta_J} \\ &+ \sum_{L\in\mathbb{Z}} \left[\sum_{l\in\mathbb{Z}} S_{L-l} B_l^{(J)} + \sum_{j\neq J} \sum_{l\in\mathbb{Z}} S_{L-l}^{(J,j)} B_l^{(j)} \right. \\ &\left. + \sum_{j\in\mathcal{N}^c} \sum_{l\in\mathbb{Z}} \sum_{q\in\mathbb{Z}} Q_{Llq}^{(J,j)} B_l^{(j)} + \sum_{q\in\mathbb{Z}} F_{qL}^{(J)} \right] J_L\left(k^{[1]}r_J\right) e^{\mathrm{i}L\theta_J} \\ = &\sum_{L\in\mathbb{Z}} \left[B_L^{(J)} \mathrm{H}_L^{(1)}\left(k^{[1]}r_J\right) + A_L^{(J)} \mathrm{J}_L\left(k^{[1]}r_J\right) \right] e^{\mathrm{i}L\theta_J}, \end{aligned} \tag{7}$$

with

$$\begin{aligned} F_{qL}^{(J)} &= \frac{2\delta_q \alpha_q^{[0]}}{D_q} \cos\left(k_{2q}^{[1]}x_2^{(J)} - L\theta_q\right) e^{\mathrm{i}k_{1q}^{[1]}x_1^{(J)}}, \\ S_{L-l} &= \sum_{i=1}^{\infty} \mathrm{H}_{L-l}^{(1)}\left(k^{[1]}id\right) \left[e^{\mathrm{i}k_1^i id} + (-1)^{L-l} e^{-\mathrm{i}k_1^i id} \right], \\ Q_{Llq}^{(J,j)} &= \frac{2(-\mathrm{i})^{l-L} e^{\mathrm{i}k_{1q}\left(x_1^{(J)} - x_1^{(j)}\right)}}{dk_{2p}^{[1]} D_q} \left[\left(\alpha_q^{[1]} - \alpha_q^{[0]}\right) e^{\mathrm{i}k_{2q}^{[1]}H} \right. \\ &\quad \times \cos\left(k_{2q}^{[1]}\left(x_2^{(j)} - x_2^{(J)}\right) - (l-L)\theta_q\right) \\ &\quad + \alpha_q^{[1]} \cos\left(k_{2q}^{[1]}\left(x_2^{(j)} + x_2^{(J)} - H\right) - (l+L)\theta_q\right) \\ &\quad \left. + \mathrm{i}\alpha_q^{[0]} \sin\left(k_{2q}^{[1]}\left(x_2^{(j)} + x_2^{(J)} - H\right) - (l+L)\theta_q\right) \right], \\ D_q &= \alpha_q^{[0]} \cos\left(k_{2q}^{[1]}H\right) - \mathrm{i}\alpha_q^{[1]} \sin\left(k_{2q}^{[1]}H\right), \end{aligned} \tag{8}$$

wherein S_{L-l} is the lattice sum often refered to as the Schlömilch series for non-dissipative material, $\mathrm{H}_L^{(1)}$ is the Lth order Hankel function of the first kind, J_L is the Lth order Bessel function, and $\alpha_q^{[j]} = k_{2q}^{[j]}/\rho^{[j]}$, $j = 0, 1$. The terms $S_{L-l}^{(J,j)}$ account for the coupling between the multiple inclusions inside the unit cell and take the form

$$\begin{aligned} S_{Ll}^{(J,j)} = &\sum_{q\in\mathbb{Z}} \frac{(-\mathrm{i})^{L-l} 2e^{\pm\mathrm{i}(L-l)\theta_q}}{dk_{2q}^{[1]}} \\ &\times e^{\mathrm{i}\left(k_{1q}\left(x_1^{(J)} - x_1^{(j)}\right) \pm k_{2q}^{[1]}\left(x_2^{(J)} - x_2^{(j)}\right)\right)} \left(1 - \delta_{Jj}\right), \end{aligned} \tag{9}$$

wherein the signs + and − correspond to $x_2^J \geq x_2^j$ and $x_2^J \leq x_2^j$, respectively, which can be found in Ref. 1 when $|x_2^{(J)} - x_2^{(j)}| > R^{(j)} + R^{(J)}$ or

$$S_{Ll}^{(J,j)} = \left[\mathrm{H}_{L-l}^{(1)}\left(r_J^j\right) e^{\mathrm{i}(l-L)\theta_J^j} + \sum_{o\in\mathbb{Z}} S_{o-l} B_l^{(j)} \mathrm{J}_{L-o}\left(k^{[1]} r_J^j\right) e^{\mathrm{i}(o-L)\theta_J^j} \right] (1-\delta_{Jj}), \tag{10}$$

when $|x_2^{(J)} - x_2^{(j)}| \leq R^{(j)} + R^{(J)}$. This latter form agrees with the one found in Ref. 15 when the inclusions are aligned inside the unit cell, i.e., $x_2^{(j)} = x_2^{(J)}$, $\forall j \in \mathcal{N}^c$, which imposes $\theta_J^j = 0$ or $\theta_J^j = \pi$. In Eq. (10), (r_J^j, θ_J^j) is the coordinate of $\mathbf{x}^{(j)}$ in the polar coordinate system attached to the Jth inclusions, i.e., centered at $\mathbf{x}^{(J)}$.

Finally, it is well known that the coefficients of the scattered field and those of the locally-incident field are linked by a matrix relation derived from the boundary condition on $\Gamma^{(J)}$ only, i.e., $B_L^{(J)} = V_L^{(J)} A_L^{(J)}$, wherein $V_L^{(J)}$ are the cylindrical harmonic reflection coefficients. These coefficients take the form $V_L^{(J)} = -\dot{\mathrm{H}}_L^{(1)}\left(k^{[1]}R^{(j)}\right)/\dot{\mathrm{J}}_L\left(k^{[1]}R^{(j)}\right)$ in the case of Neumann type boundary conditions, with $\dot{\chi}(x) = d\chi/dx$, χ being either Hankel or Bessel functions. Introducing the expression of $A_L^{(J)}$ derived from Eq. (7) in the previous relation gives rise to the linear system of equations for the solution of $B_L^{(j)}$. This linear system may be written in the matrix form, where $\mathbf{B}$ denotes the infinite column matrix of components $B_L^{(j)}$,

$$(\mathbf{I} - \mathbf{V}(\mathbf{S} + \mathbf{Q}))\mathbf{B} = \mathbf{V}\mathbf{F}, \tag{11}$$

wherein $\mathbf{I}$ is the identity matrix and $\mathbf{F}$ is a vector of components $\sum_{q\in\mathbb{Z}} F_{qL}^{(J)}$. This accounts for the solicitation of the Jth inclusion by a wave that is previously diffracted inside the layer. $\mathbf{V}$ is a diagonal square matrix of components $V_L^{(J)}$. $\mathbf{S}$ and $\mathbf{Q}$ are two matrices of components $S_{L-l} + S_{L-l}^{(J,j)}$, which account for the coupling between the J-th and the j-th inclusion inside the layer, and $\sum_{q\in\mathbb{Z}} Q_{Llq}^{(J,j)}$ accounts for the coupling between the Jth and the jth inclusion through waves diffracted by the layer.

The expressions of the components involved in $(\mathbf{I} - \mathbf{V}(\mathbf{S} + \mathbf{Q}))\mathbf{B} = \mathbf{V}\mathbf{F}$ are identical to those found in Ref. 1, when the half-space behind the layer vanishes and when the center of the cylinders are defined as they are in the present article.

C. Evaluation of the fields, reflection and absorption coefficients

Once the linear system (11) is solved, the expression of R_q in terms of $B_l^{(j)}$ reads as

$$R_q = \frac{\alpha^{[0]i}\cos\left(k_2^{[1]i}L\right) + \mathrm{i}\alpha^{[1]i}\sin\left(k_2^{[1]i}L\right)}{D^i} + \sum_{q\in\mathbb{Z}}\sum_{j\in\mathcal{N}^c}\sum_{l\in\mathbb{Z}} \frac{4(-\mathrm{i})^l \alpha_q^{[1]}}{dk_{2q}^{[1]} D_q} B_l^{(j)} \cos\left(k_{2q}^{[1]} x_2^{(j)} - l\theta_q\right) e^{-\mathrm{i}k_{1q}x_1^{(j)}}. \tag{12}$$

The first term corresponds to the reflection coefficient in terms of waves in absence of inclusion, i.e., for $q = 0$ or for the incident plane component indexed by i, and the second term accounts for the inclusions.

Introduced in Eq. (5), the reflected field is expressed as a sum of the field with inclusions and without. In case of an incident plane wave with spectrum $A^i(\omega)$, the conservation of energy relation takes the form

$$1 = \mathcal{R} + \mathcal{A}, \tag{13}$$

with $\mathcal{R}$ and $\mathcal{A}$ the hemispherical reflection and absorption coefficients, respectively. $\mathcal{R}$ is defined by

$$\mathcal{R} = \sum_{q\in\mathbb{Z}} \frac{\mathrm{Re}\left(k_{2q}^{[0]}\right)}{k_2^{[0]i}} \frac{\| R_q \|^2}{\| A^i \|^2} = \sum_{q=-\tilde{q}}^{\tilde{q}_+} \frac{k_{2q}^{[0]}}{k_2^{[0]i}} \frac{\| R_q \|^2}{\| A^i \|^2}, \tag{14}$$

wherein $\tilde{q}_\mp$ are such that $\tilde{q}_\mp < d/2\pi\left(k^{[0]} \pm k_1^i\right) < \tilde{q}_\mp + 1$ and the expression of R_q are given by Eq. (12). $\mathcal{A}$ takes the form[6]

$$\mathcal{A} = \frac{1}{dk_2^{[0]i}\,\| A^i \|^2} (\mathcal{A}_D + \mathcal{A}_S), \tag{15}$$

wherein

$$\mathcal{A}_D = \frac{\rho^{[0]}}{\mathrm{Re}(\rho^{[1]})} \int_{\Omega_{[1]}} \mathrm{Im}\left(\left(k^{[1]}\right)^2\right) \| p^{[1]}(\mathbf{x}) \|^2 \, \mathrm{d}\bar{\omega} \tag{16}$$

is the inner absorption of domain $\Omega^{[1]}$. $\mathrm{d}\bar{\omega}$ is the differential element of surface in the sagittal plane and

$$\mathcal{A}_S = \mathrm{Re} \int_{\Gamma_H} \frac{\rho^{[0]}}{\rho^{[1]}} \frac{\mathrm{Im}\left(\rho^{[1]}\right)}{\mathrm{Re}\left(\rho^{[1]}\right)} p^{[1]*}(\mathbf{x}) \nu_{01} \cdot \nabla p^{[1]}(\mathbf{x}) \mathrm{d}\gamma \tag{17}$$

is the surface absorption related to interfaces Γ_H. $\mathrm{d}\gamma$ is the differential arc length in the cross-sectional plane, ν_{01} is the outward-pointing unit vector to the boundary Γ_H, and p^* is the complex conjuguate of p.

$\mathcal{A}_S$ accounts for the absorption induced by the viscous dissipation at the interfaces. Indeed, it is obvious from Eq. (17) that $\mathcal{A}_S$ does not vanish because of the presence of Im $(\rho^{[1]})$, which is a consequence of the modeling of viscous dissipation phenomenon.[17]

Because of the complicated shape of $\Omega^{[1]}$ and the non-vanishing term $\mathcal{A}_S$ $\mathcal{A}$ will not be calculated by the expression given in Ref. 15, but rather by $\mathcal{A} = 1 - \mathcal{R}$.

IV. NUMERICAL RESULTS, VALIDATION AND DISCUSSION

The infinite sum $\sum_{q\in\mathbb{Z}}$ over the indices of k_{1q} depends on the frequency and on the period of the grating. An empirical truncation rule is employed, as in Refs. 1, 2, and 6, and determined by performing a large number of numerical experiments $\sum_{q=-Q_-}^{Q_+}$ such that $Q_\mp = \mathrm{int}\left(d/2\pi\left(3\mathrm{Re}\left(k^{[1]}\right) \pm k_1^i\right)\right) + 10$. In these equations, int(a) represents the integer part of a.

The infinite sum $\sum_{m\in\mathbb{Z}}$ over the indices of the modal representation of the diffracted field by a cylinder is

truncated[18] as $\sum_{m=-M}^{M}$, such that $M = \text{int}(\text{Re}(4.05 \times (k^{[1]}R)^{1/3} + k^{[1]}R)) + 10$.

Finally, the infinite sum (lattice sum) embedded in S_{L-l} in Eqs. (8) and (10) $\sum_{i=1}^{\infty}$ is found to be slowly convergent, particularly in the absence of dissipation, and is found to be strongly dependent on the indice $L-l$. A large literature exists on this problem.[19,20] Here, the fact that the medium $M^{[1]}$ is dissipative greatly simplifies the evaluation of the Schlömilch series. The superscript I in $S_{L-l}^{\{I\}}$ identifies the integer over which the sum is performed, i.e., $\sum_{i=1}^{I}$. This sum is carried out until the conditions $\left|\text{Re}\left(\left(S_{L-l}^{\{I+1\}} - S_{L-l}^{\{I\}}\right)/S_{L-l}^{\{I\}}\right)\right| \leq 10^{-5}$ and $\left|\text{Im}\left(\left(S_{L-l}^{\{I+1\}} - S_{L-l}^{\{I\}}\right)/S_{L-l}^{\{I\}}\right)\right| \leq 10^{-5}$ are reached.[2]

Numerical calculations have been performed for various geometrical parameters whose values are reported in Table I, and within the frequency range of audible sound, particularly at low frequencies. For all calculations, the ambient and saturating fluid is air ($\rho^{[0]} = \rho_f = 1.213\,\text{kg m}^{-3}$, $c^{[0]} = \sqrt{\gamma P_0/\rho_f}$, with $P_0 = 1.01325 \times 10^5\text{Pa}$, $\gamma = 1.4$, and $\eta = 1.839 \times 10^{-5}\,\text{kg m}^{-3}\,\text{s}^{-1}$). Two of the main constraints in designing acoustically absorbing materials are the size and weight of the configuration. Particular attention is placed on the thickness and the frequencies of the absorption gain, which have to be as small as possible. The absorption gain is defined in reference to the absorption of the same configuration without inclusion embedded. The initial configuration consists in a 2 cm thick porous sheet of Fireflex (Recticel, Belgium) backed by a rigid plate. The material characteristics are reported in Table II and were determined by use of methods described in Refs. 11, 21–23. Circular cylinders of 7.5 mm radius are embedded with a spatial periodicity of 2 cm. As mentioned in Sec. II A, the inclusions can be constituted of various material (or geometries like tubes), while the outside boundary is circular and can be modeled with a Neumann type boundary condition.

A. One inclusion per spatial period

We first consider only one inclusion centered in the unit cell, i.e., $(x_1^{(1)}, x_2^{(1)}) = (d/2, H/2) = (1\,\text{cm}, 1\,\text{cm})$. The first two modified modes of the plate, which are excited because of the periodic arrangement of the inclusions, Appendix A, have frequencies $\nu_{(1,1)} \approx 14\,\text{kHz}$ and $\nu_{(2,1)} \approx 16\,\text{kHz}$. The attenuation associated with both modes is relatively large (see Fig. 3).

Different types of waves correspond to each kind of mode related to the grating, i.e., mode of the grating (MG) and modified mode of the backed layer (MMBL): evanescent waves in $\Omega^{[1]}$ (and also in $\Omega^{[0]}$) for the MG, and evanescent waves in $\Omega^{[0]}$ and propagative waves in $\Omega^{[1]}$ for the MMBL. In order to determine which type of mode is excited by the plane incident wave, we have plotted in Fig. 2 the transfer function as calculated by $\text{TF}(\nu) = p(\mathbf{x},\nu)/p^{[0]i}(\mathbf{x},\nu)$ on Γ_0 ($x_2 = 0$) at 1 cm from the center of the inclusion (between two inclusions), when excited at normal incidence. The transfer function is separated on the different intervals corresponding to the different type of waves that are involved in the total pressure calculation: $\text{TF}(\nu)$ is the total transfer function, $\text{TF}_1(\nu)$ is the contribution of the propagative waves in both $\Omega^{[0]}$ and $\Omega^{[1]}$, $\text{TF}_2(\nu)$ is the contribution of the evanescent waves in $\Omega^{[0]}$ and propagative ones in $\Omega^{[1]}$, and $\text{TF}_3(\nu)$ is the contribution of the evanescent waves in both $\Omega^{[0]}$ and $\Omega^{[1]}$. The transfer function possesses a large peak at $\approx 15\,\text{kHz}$, around $\nu_{(1,1)}$ and $\nu_{(2,1)}$. This also proves that the MMBL are the most excited modes, related to the grating, around these frequencies. The peak results from a continuous transition between evanescent waves in both materials to evanescent waves in the air medium (around 13 kHz, Fig. 2). This also means that this peak is neither a MMBL nor a MG, but results from a complex combination of these two types of modes, with a structure closer to that of the MMBL. Because of this structure, the energy is trapped in the layer, leading to an increase in the absorption coefficient. The translation of the excitation of these modes in terms of absorption, i.e., the peak around 17 kHz in Fig. 3, is smaller than the one depicted in Ref. 6, because (i) the attenuation associated with the modes in the present configuration is larger, and (ii) the static flow resistivity of the foam considered here is larger. The design of a structure composed of a layer with inclusions embedded is more based on compromises than with irregularities of the rigid backing.[6] These compromises relate the spatial periodicity, the radius of the

TABLE I. Geometry of the considered configurations.

	N	d (cm)	H (cm)	$(x_1^{(j)}(\text{cm}),\ x_2^{(j)}(\text{cm}))$	$R^{(j)}$ (cm)
C1	1	2	2	(1,1)	0.75
C2	2	2	3.5	$(x_1^{(1)}, x_2^{(1)}) = (1,1)$	$R^{(1)} = 0.75$
				$(x_1^{(2)}, x_2^{(2)}) = (0.5, 1+\sqrt{3}d/2)$	$R^{(2)} = 0.5$

TABLE II. Parameters of the porous foam used in the article.

ϕ	α_∞	Λ (μm)	Λ' (μm)	σ (N s m^{-4})	v_c (Hz)
0.95	1.42	180	360	8900	781

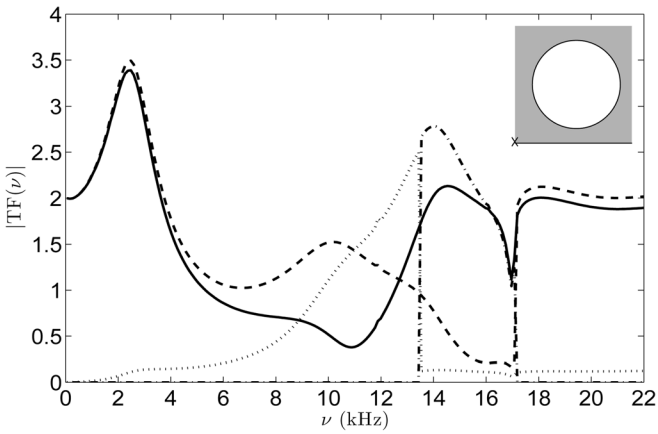

FIG. 2. Configuration C1 – Transfer function, TF (–), on Γ_0 at 1 cm from the center of the inclusion (between two inclusions), and its different contributions when the configuration is excited at normal incidence: (––) TF_1, (–·) TF_2, and (··) TF_3.

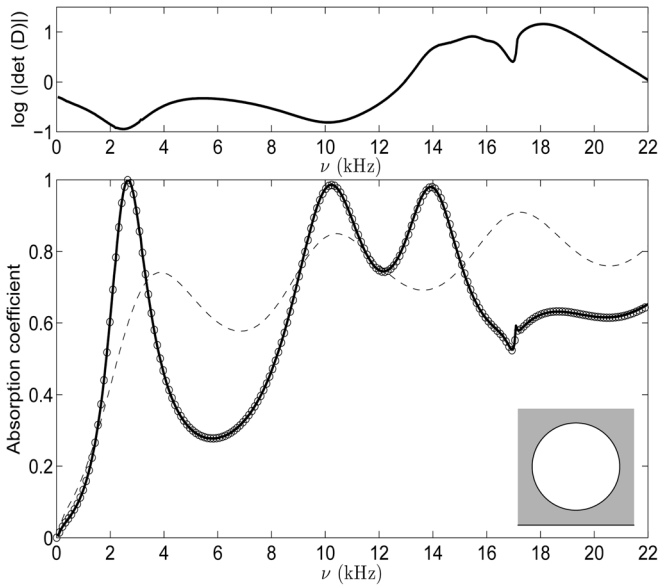

FIG. 3. Configuration C1 – Absorption coefficient of a $H = 2$ cm thick porous sheet of Fireflex backed by a rigid plate (– – –) without inclusion embedded and (–) with a $R = 7.5$ mm radius circular cylinder embedded per spatial period $d = 2$ cm, when the configuration is excited at normal incidence. The Finite Element result is plotted with (o). The absolute value of the determinant of the propagation matrix $\mathbf{D} = \mathbf{I} - \mathbf{V}(\mathbf{S} + \mathbf{Q})$ is plotted on top of the figure.

inclusion, or better, the ratio R/d, which cannot be too small and which constrains the layer thickness and the properties of the latter.

Figure 3 depicts the absorption coefficient calculated for this geometry. This result was validated numerically by matching the absorption coefficient calculated with the present method with the one calculated with a finite element method. Quadratic finite elements were used to approximate the pressure inside the unit cell, thereby leading to a discretized problem of 2196 elements and 1238 nodes. The periodicity relation, i.e., the Floquet condition, was applied on both sides of the discretized domain, i.e., at each nodes of x_1-coordinate 0 and d. For this periodicity relation to be correctly implemented, these two sides were discretized with similar nodes, i.e., identical x_2-coordinates. The results match well, thus validating the described method (see Fig. 3). When compared to the finite element method, the mode-matching technique enables analytic calculations and is less time consuming (approximatively a quarter of the time) for the configurations and frequency range considered in this article. This is due to the fact that the dimensions and frequency range considered therein enable to account only for a small number of terms in the infinite sums over m, q, and for the correct evaluation of the lattice sum.

Because of the rigid backing, which acts as a perfect mirror, the response of the configuration possesses some particular features related to multi-layered grating. We also introduce $d_2 = 2x_2^{(1)}$, the distance between the center of the circular cylinder and the center of its image. Each grating interferes with one another at the Bragg frequencies $\nu^b_{(n)} = n\mathrm{Re}\left(c^{[1]}\right)/2d_2$. In particular, the first Bragg frequency, $\nu^b_{(1)} \approx 6$ kHz, is largely employed to determine the central frequency of the band gaps for phononic crystals corresponding to a maximum of reflected energy and to a minimum of transmitted energy—band gaps—in case of phononic crystal. The absorption coefficient also presents a minimum at $\nu^b_{(1)}$.

A particular feature of the response of this configuration is that the absorption coefficient presents a peak close to unity at a low frequency ν_t below the so-called fundamental quarter-wave resonance frequency, i.e., below what can be associated with an essential spectrum.

A sensitivity analysis, performed by varying one parameter while the others are kept constant at value, shows that the radius of the inclusion has a large influence on ν_t and on the amplitude of the corresponding absorption peak. The radius R was varied from 1.5 mm to 9.5 mm, Fig. 4(a). In terms of amplitude of the absorption peak, $R = 7.5$ mm is the optimal value, while ν_t decreases when R increases. In contrast, $d = 2$ mm is the optimal value in terms of the peak amplitude, but ν_t increases when d increases from 1.75 cm to 3.75 cm. The spatial periodicity of the arrangement acts inversely on ν_t than it does on the frequencies of the modes closely related to d like the MMBL and the MG, Appendix.

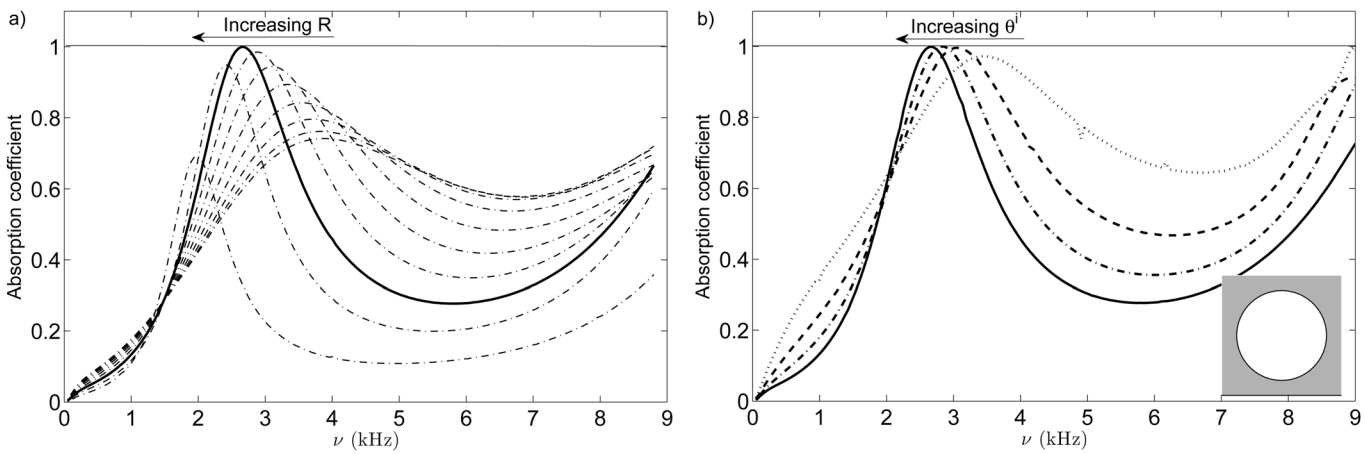

FIG. 4. Configuration C1 – Absorption coefficient of a $H = 2$ cm thick porous sheet of Fireflex backed by a rigid plate (a) for a radius R increasing from 1.5 mm to 9.5 mm (with a step of 1 mm) circular cylinder embedded per spatial period $d = 2$ cm, when the configuration is excited at normal incidence, and (b) for $R = 7.5$ mm radius circular cylinder embedded per spatial period $d = 2$ cm, when the configuration is excited at $\theta^i = \pi/2$ (-), $\theta^i = \pi/3$ (– · –), $\theta^i = \pi/4$ (– – –), and $\theta^i = \pi/6$ (· · ·).

In fact, the amplitude of the absorption peak increases with the filling ratio R/d until being close to unity and drastically decreases after this value. This is either because the wave can no longer propagate in the layer towards the rigid backing and is mainly reflected on the circular grating, or because the density of inclusion becomes insignificant. In the same way, when the angle of incidence decreases $[\pi/2;\pi/6]$, the ν_t increases in opposition to the frequencies of the MMBL and of the MG. The amplitude of the peak is quite close to unity until $\pi/6$. For smaller values of incidence angle, the amplitude of this low frequency peak begins to decrease, Fig. 4(b).

When $R = 7.5$ mm and $d = 20$ mm, ν_t is all the smaller that the inclusion is distant from the rigid backing, i.e., that $x_2^{(1)}$, the center of the inclusion, is large. The amplitude of the peak is close to unity whatever $x_2^{(1)}$, in $[0.8\,\text{cm}; 1.2\,\text{cm}]$ the range conditioned by the layer thickness and the inclusion radius.

The features of this low frequency absorption peak ressembles phenomena that are related to trapped modes in waveguides[9] or embedded Rayleigh-Bloch waves.[10,24] These modes have finite energy and correspond to a solution which decays down away from the perturbation. Figure 5 shows a snapshot of the module of the pressure field at ν_t. This clearly exibits a maximum on the side of the rigid plate and a minimum on the side of Γ_0, which is typical of a trapped mode. Everything seems to happen as if a Dirichlet waveguide of thickness $2H$ presents symmetric obstacles formed by the inclusion and its image. In our case, these trapped modes are complex, because the boundaries of the waveguide are not Dirichlet conditions but Neumann and continuity conditions, and because $M^{[1]}$ is a dissipative medium. The determinant as calculated for the configuration C1, Fig. 3, presents a minimum at ν_t, which suggests that a complex (trapped) mode CTM stands at this frequency. In contrast, it is clear from Fig. 2, that the peak around ν_t is mainly associated with propagative waves in both domains, a small part of it being associated with evanescent waves in the layer which entraps the energy. This phenomena was already encountered in Ref. 25 and attributed to the periodicty of the configuration. Another explanation of the quasi-absorption peak is related to the modification of wave path and structure global properties inside the porous sheet. For a particular ratio R/d, the pressure gradient and thereby the velocity, which is a cause of viscous loss, is large between the inclusions and between the inclusions and the rigid backing. This loss phenomenon results from a continuous modification of the quarter-wavelength resonance when the inclusion radius increases.

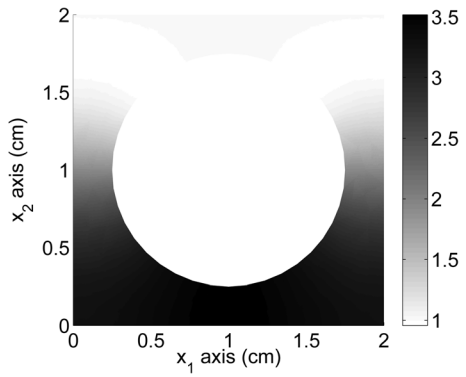

FIG. 5. Configuration C1 – Snapshot of the module of the pressure field inside the porous sheet at $\nu_t = 2674$ Hz, when the configuration is excited at normal incidence.

Other layer thicknesses were tested. It was found that for most of the layer thickness, in the suitable range for the application, and a centered $(x_1^{(1)}, x_2^{(1)}) = (d/2, H/2)$ inclusion, a couple (R, d) exists for which a quasi-total absorption peak exists below the quarter-wavelength resonance frequency.

Finally, because the parameters of a foam are often difficult to predict before its polymerization, a sensitivity analysis has been performed with regards to the acoustic and structural parameters of the porous sheet. Each parameter of the porous foam is varied one after the other, while keeping the other constant at their value as shown in Table II. Each parameter is assumed to be independent from the other, but their variations correspond to those encountered in practice. The amplitude and frequency of the absorption peaks are weakly dependent on a variation of ϕ ($[0.85; 0.95]$), Λ ($[160\ \mu\text{m}; 200\ \mu\text{m}]$) and Λ' ($[300\ \mu\text{m}; 420\ \mu\text{m}]$). In particular, the amplitude (more than 0.98) and frequency (a shift of a few decade of Hz) of the CTM is quasi independent of a variation of these parameters. When α_∞ increases from 1.02 to 1.42, the sound speed in the material decreases and ν_t decreases, while the amplitude of the associated peak stands close to one. The static flow resistivity σ strongly influences the amplitude of the peak. When it increases, the amplitude admits a maximum and the peak is wider, while ν_t increases. The resistivity σ ($[3900\ \text{N s m}^{-4}; 12\,900\ \text{N s m}^{-4}]$) is the parameter that mostly influences the results, and its value has to be close to the one used in the simulations, i.e., in our case, a value between $7000\ \text{N s m}^{-4}$ and $11\,000\ \text{N s m}^{-4}$ is acceptable.

B. Two or more inclusions per spatial period

Various configurations were tested, involving two or more inclusions per spatial period. The frequency band investigated stands below the quarter-wavelength resonance frequency of the associated porous sheet or at least below the first Bragg frequency, i.e., below the frequency of the first modified mode of the porous sheet. The lowest frequency bound is naturally the solid-fluid decoupling frequency or at least the Biot frequency.

Two absorption peaks close to unity were found for a $H = 3.5$ cm thick porous sheet, when a second circular cylinder of radius $R^{(2)} = 5$ mm is added to the configuration C1, Fig. 6. The center of this cylinder is such that $r_1^2 = d = 2$ cm and $\theta_1^2 = \pi/3$. The configuration C2 was derived from a triangular lattice by reducing the radius of the upper cylinder to decrease the structure thickness. The first absorption peak stands around $\nu_t^{(1)} \approx 1850$ Hz, just below the first quarter-wavelength resonance frequency of the $H = 3.5$ cm thick porous sheet, and the second stands around $\nu_t^{(2)} \approx 4120$ Hz. These two peaks correspond to a minimum of $|\det(\mathbf{D})|$ and can therefore be explained by excitation of trapped modes, shifted in the complex plane.

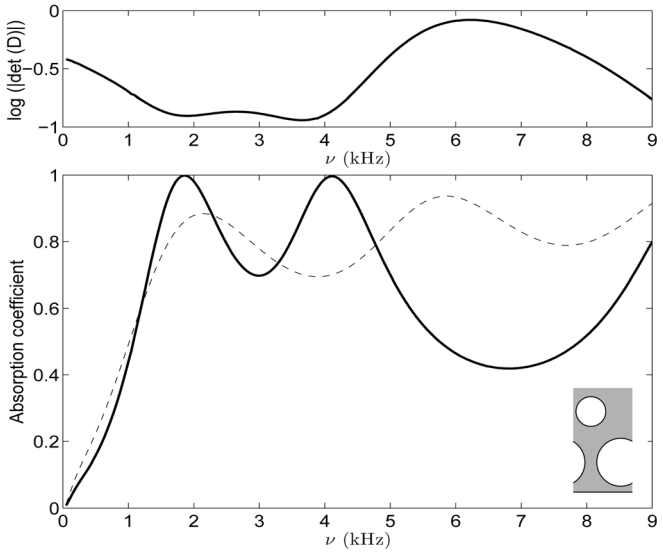

FIG. 6. Configuration C2 – Absorption coefficient of a $H = 3.5$ cm thick porous sheet of Fireflex backed by a rigid plate (– – –) without inclusion embedded and (-) with a $R^{(1)} = 75$ mm radius circular cylinder and a $R^{(2)} = 5$ mm radius circular cylinder embedded with $d = 2$ cm, when the configuration is excited at normal incidence.

When the inclusions are inversely placed, i.e., the center of the first inclusion is (1 cm, 2.5 cm) and $r_1^2 = d = 2$ cm and $\theta_1^2 = -\pi/3$, results are not identical and no quasi-total absorption peak is encountered. This means that the configuration is not reversible.

The procedure was run a second time with the addition of a third inclusion of radius $R^{(3)} = 2.5$ mm to the configuration C2, $r_2^3 = d = 2$ cm and $\theta_2^3 = 2\pi/3$. Three quasi-total absorption peaks were encountered around $\nu_t^{(1)} \approx 1500$ Hz, $\nu_t^{(2)} \approx 3300$ Hz, and $\nu_t^{(3)} \approx 5000$ Hz.

This phenomenon was already encountered in Ref. 26, where N trapped modes were found when N cylinders were placed across a wave tank. Nevertheless, this configuration imposes use of $H = 5$ cm thick plate, and the absorption gain was considered insignificant over the whole frequency range considered. The addition of inclusions that imposes a thickening of the structure is rapidly becoming of no practical use because of the large absorption of the porous layer itself.

Based on the fact that the frequency $\nu_t^{(1)}$ decreases when $x_2^{(1)}$ increases, several attempts were followed to construct a porous sheet with a unit cell composed of varying $x_2^{(j)}$ central coordinate circular cylinder arranged in a kind of garland. For example, the absorption coefficient of eight circular cylinders per unit cell, embedded in a 2 cm thick porous sheet, was studied. The radius of the eight cylinders was $R^{(j)} = 75$ mm and the projection of the center-to-center distance between two adjacent cylinders $x_1^{(j,j+1)}$ was 2 cm. The $x_2^{(j)}$ were chosen such that $x_2^{(1)} = 1.1$ cm, $x_2^{(2)} = 1.05$ cm, $x_2^{(3)} = 1$ cm, $x_2^{(4)} = 0.95$ cm, $x_2^{(5)} = 0.9$ cm, $x_2^{(6)} = 0.95$ cm, $x_2^{(7)} = 1$ cm, and $x_2^{(8)} = 1.05$ cm. The absorption peak at ν_t was no more total, and no particular increase of its width was noticed. This means that the periodicity has a large influence on the results and that the phenomenon cannot be simply explained by trapped modes but rather by complex embedded Rayleigh-Bloch waves. A similar procedure was followed by decreasing the radius and the center-to-center distance, the cylinders being aligned, without particular effects on the absorption.

V. CONCLUSION

The influence of embedding periodic circular inclusions on the absorption of a porous sheet attached to a rigid plate was studied theoretically and numerically. In addition to the absorption features related to the excitation of modified modes of the plate and to Bragg interference, it is shown that the structure can possess a quasi-total (close to unity) absorption peak below the quarter-wavelength resonance frequency. This occurs in case of one array of cylinders embedded in a porous sheet, whose thickness and parameters, mainly the static flow resistivity, are correctly chosen. This particular feature enables the design of small dimension absorption packages and was explained by complex trapped mode excitation, which leads to an increase of the pressure gradient inside the layer. This quasi-total absorption peak was validated by use of the finite element method, thus validating the described method and results.

In case of more than one circular cylinder per spatial period, it was found that the N^c quasi-total absorption peak can be obtained for a particular arrangement along the porous thickness, i.e., close to triangular lattice. Nevertheless, this rapidly leads to a large thickness of the structure, and the embedding of the additional inclusions become useless. Garland arrangements were also tested without particular effect, or at least without as spectacular effect as the one already observed for one inclusion per spatial period.

The method offers an alternative to multi-layering and double porosity materials for the design of sound absorption packages. Nevertheless, accounting for the full Biot theory to model the behavior of the porous sheet and the possible coupling between the frame and the inclusions, would be of large interests for lower frequency applications.

ACKNOWLEDGMENT

The authors would like to thank Matthew Boucher for his useful help during the writing of the paper. We are saddened by the sudden death (September 19, 2010) of our highly respected colleague Walter Lauriks, to whom we are very grateful for the important inspiration he shared with us in relation to this work.

APPENDIX: MODAL ANALYSIS OF THE CONFIGURATION

The modes of the configuration without inclusions embedded (i.e., a rigid porous layer backed with a planar rigid wall), whose dispersion relation is

$$D^i = \alpha^{[0]i} \cos\left(k_2^{[1]i} H\right) - \mathrm{i}\alpha^{[1]i} \sin\left(k_2^{[1]i} H\right) = 0, \qquad \text{(A1)}$$

wherein $\alpha_0^{[j]} = \alpha^{[j]i}$, $j = 0, 1$, and $k_{20}^{[1]} = k_2^{[1]i}$, $j = 0, 1$, cannot be excited by a plane incident wave initially traveling in the air medium.[6] Effectively, Fig. 7 depicts the real and the

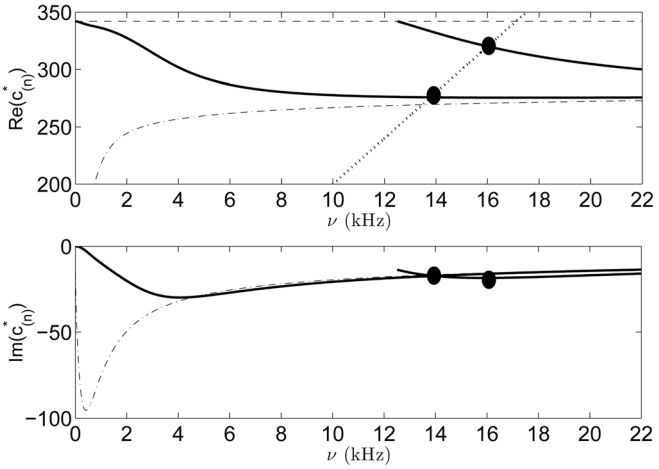

FIG. 7. Real and imaginary part of the root of the dispersion relation in absence of inclusions $c^*_{(n)}$, $n = 1, 2$ (–), of the sound speed in air (−−), and of the sound speed in the homogeneous porous material (−·). Real part of the modified mode of the backed layer $c^*_{(n,q)}$, $n = 1, 2$, $q = 1, 2$, for $d = 2$ cm are pointed out by dot.

imaginary parts of the roots $c^*_{(n)}(\omega) = \omega/k^*_{1,(n)}(\omega)$ of Eq. (A1), as calculated for a $H = 2$ cm thick porous layer, whose acoustical characteristics are those used in Sec. IV. Under the rigid frame assumption and for frequencies higher than the Biot frequency (and lower than the diffusion limit), a porous material can be considered as a modified fluid, its associated dissipation being considered as a perturbation of a fluid. For Eq. (A1) to be true without dissipation, $k_2^{[0]\,i}$ should be purely imaginary while $k_2^{[1]\,i}$ should be purely real. Under the previous assumptions, this implies that $\mathrm{Re}(c^*_{(n)})$ should stand in $[\mathrm{Re}(c^{[1]}), c^{[0]}]$, i.e., $|k_1^i|$ should stand in $[k^{[0]}; \mathrm{Re}(k^{[1]})]$. Or for a plane incident wave initially propagating in the air medium $|k_1^i|$ is always smaller than $k^{[0]}$. It is also necessary to note that in the diffusion regime, i.e., for frequencies largely below the Biot Frequency, any mode exists. This fact constitutes the major difference when compared with a traditional fluid. Effectively, largely below the Biot frequency, $k^{[1]}$ is purely imaginary. This implies that $k_2^{[1]\,i}$ is also purely imaginary for all values of k_1^i and that D^i never vanishes.

When inclusions are periodically embedded in the porous sheet, the dispersion relation of the modes of the configuration is $\det(\mathbf{I} - \mathbf{V}(\mathbf{S} + \mathbf{Q})) = 0$. The roots of this dispersion relation are difficult to determine because of the complex nature of the matrix $\mathbf{I} - \mathbf{V}(\mathbf{S} + \mathbf{Q})$. Here, we focus on the case of only one grating, i.e., $N^c = 1$, in order emphasize the excitation of the modified mode of the backed layer (MMBL) (Ref. 6). Proceeding as in Ref. 2, an iterative scheme can be employed to solve.[11] The equation is re-written in the form $(1 - V_L\mathcal{M}_{LL})B_L = V_L\mathcal{F}_L + V_L\sum_{l\in\mathbb{Z}} \mathcal{M}_{Ll}B_l(1 - \delta_{Ll})$. The iterative scheme reads as

$$\begin{cases} B_L^{\{0\}} & = V_L\mathcal{F}_L/(1 - \mathcal{M}_{LL}) \\ B_L^{\{n+1\}} & = \left(V_L \sum\limits_{l\in\mathbb{Z}} \mathcal{M}_{Ll}B_l^{\{n\}}(1 - \delta Ll) + V_L\mathcal{F}_L\right) \Big/ \\ & \quad (1 - V_L\mathcal{M}_{LL}), \end{cases} \tag{A2}$$

from which it becomes apparent that the solution $B_L^{\{n\}}$, to any order of approximation, is expressed as a fraction, the denominator of which not depending on the order of approximation can become small for certain couples (k_{1q}, ω), so as to make $B_L^{\{n\}}$, and possibly the field large.

When this happens, a natural mode of the configuration, comprising the inclusions and the plate, is excited, thus taking the form of a resonance with respect to $B_L^{\{n\}}$, i.e., with respect to a plane wave component of the field in the plate relative to the inclusions. As $B_L^{\{n\}}$ is related to f_q, g_q, and R_q, the structural resonance manifests itself for the same (k_{1q}, ω), in the fields of the plate and in the air.

The approximate dispersion relation

$$\mathcal{D}_L = 1 - V_L\left(S_0 + \sum_{q\in\mathbb{Z}} Q_{LLq}\right) = 0, \tag{A3}$$

is the sum of a term linked to the grating embodied in V_LS_0 with a term linked to the plate embodied in $V_L\sum_{q\in\mathbb{Z}} Q_{LLq}$, whose expressions are given in Eq. (8).

This can be interpreted as a perturbation of the dispersion relation of the gratings by the presence of the plate. The zeroth order lattice sum can be rewritten[20] in the form $\sum_{q\in\mathbb{Z}} 2/dk_{2q}^{[1]}$ (additional constants are neglected). Introducing this expression into (A3) gives

$$\mathcal{D}_L = 1 - V_L \sum_{q\in\mathbb{Z}} \frac{2\mathcal{N}_{Lq}}{dk_{2q}^{[1]}D_q} = 0, \tag{A4}$$

with

$$\begin{aligned} \mathcal{N}_{Lq} = {} & \alpha_q^{[1]} \cos\left(k_{2q}^{[1]}H\right) - \mathrm{i}\alpha_q^{[1]} \sin\left(k_{2q}^{[1]}H\right) \\ & + \alpha_q^{[1]} \cos\left(k_{2q}^{[1]}\left(2x_2^{(1)} - H\right) - 2L\theta_q\right) \\ & + \mathrm{i}\alpha_q^{[0]} \sin\left(k_{2q}^{[1]}\left(2x_2^{(1)} - H\right) - 2L\theta_q\right). \end{aligned} \tag{A5}$$

It is then convenient, for the clarity of the explanations, to consider (i) $M^{[1]}$ to be a non-dissipative medium (a perfect fluid) and (ii) the low frequency approximation of V_L, valid when $k^{[1]}R^{(1)} \ll 1$. The latter hypothesis ensures that the V_L reduces to $V_l \approx (-1)^l\pi(k^{[1]}R^{(1)})^2/\mathrm{i}4 + O\left((k^{[1]}R^{(1)})^2\right)$, $l = -1, 0, 1$. Equation (A4) then reduces to

$$\mathcal{D}_l \approx 1 - \sum_{q\in\mathbb{Z}} \frac{(-1)^l(k^{[1]}R^{(1)})^2}{2\mathrm{i}dk_{2q}^{[1]}D_q/\mathcal{N}_{lq}} = 0, \quad l = -1, 0, 1. \tag{A6}$$

By referring to the Cutler mode,[27] but also to the modal analysis carried out in Ref. 2, the latter dispersion relation is satisfied (in the non-dissipative case) when the denominator of Eq. (A6) is purely imaginary and vanishes. These conditions are achieved when $|k_{1q}| \in [k^{[0]}, \mathrm{Re}(k^{[1]})]$ and when either $D_q = 0$ or $\alpha_q^{[1]} = 0$ (i.e., $k_{2q}^{[1]} = 0$), which respectively corresponds to modified modes of the backed-layer (MMBL) and to modes of the grating (MG). Both of them are determined by the intersection of $c_{1q} = \omega/k_{1q}$ respectively with $c^*_{(n)}(\omega)$

as calculated for the backed-layer and with $\mathrm{Re}\left(c^{[1]}\right)$. The MMBL are pointed out by the dots in Fig. 7. The associated attenuation of each mode can then be determined by the values of $\mathrm{Im}\left(c^{*}_{(n)}\right)$ and $\mathrm{Im}\left(c^{[1]}\right)$ at the frequencies at which the modes are excited. The attenuation associated with MG is also higher than the one associated with MMBL for all frequencies. Moreover, MG corresponds to the highest boundary of $|k_{1q}|$ for Eq. (A6) to be true. This implies that MG should be difficult to excite. The latter type of mode can only be poorly excited by a plane incident wave, particularly at low frequencies.

[1]J.-P. Groby, E. Ogam, and A. Wirgin, "Acoustic response of a periodic distribution of macrosocopic inclusions within a rigid frame porous plate," Waves Random Complex Media **18**, 409–433 (2008).
[2]J.-P. Groby, A. Wirgin, L. De Ryck, W. Lauriks, Y. X. U., and R. Gilbert, "Acoustic response of a rigid frame porous medium plate with a periodic set of inclusions," J. Acoust. Soc. Am. **126**, 685–693 (2009).
[3]V. Tournat, V. Pagneux, D. Lafarge, and L. Jaouen, "Multiple scattering of acoustic waves and porous absorbing media," Phys. Rev. E **70**, 026609 (2004).
[4]E. Gourdon and M. Seppi, "On the use of porous inclusions to improve the acoustical response of porous materials: Analytical model and experimental verification," Appl. Acoust. **71**, 283–298 (2010).
[5]X. Olny and C. Boutin, "Acoustic wave propagation in double porosity media," J. Acoust. Soc. Am. **113**, 73–89 (2003).
[6]J.-P. Groby, W. Lauriks, and T. Vigran, "Total absorption peak by use of a rigid frame porous layer backed by a rigid multi-irregularities grating," J. Acoust. Soc. Am. **127**, 2865–2874 (2010).
[7]B. Sapoval, B. Hebert, and S. Russ, "Experimental study of a fractal acoustical cavity," J. Acoust. Soc. Am. **105**, 2014–2019 (1999).
[8]B. Sapoval, S. Felix, and M. Filoche, "Localisation and damping in resonators with complex geometry," Eur. Phys. J. **161**, 225–232 (2008).
[9]C. Linton and P. McIver, "Embedded trapped modes in water waves and acoustics," Wave Motion **45**, 16–29 (2007).
[10]R. Porter and D. Evans, "Embedded rayleigh-bloch surface waves along periodic rectangular arrays," Wave Motion **43**, 29–50 (2005).
[11]J.-F. Allard and N. Atalla, *Propagation of Sound in Porous Media: Modelling Sound Absorbing Materials* (Wiley, Chichester, 2009), Chap. 5, pp. 73–107.
[12]L. De Ryck, J.-P. Groby, P. Leclaire, W. Lauriks, A. Wirgin, C. Depollier, and Z. Fellah, "Acoustic wave propagation in a macroscopically inhomogeneous porous medium saturated by a fluid," Appl. Phys. Let. **90**, 181901 (2007).
[13]Y. Champoux and J.-F. Allard, "Dynamic tortuosity and bulk modulus in air-saturated porous media," J. Appl. Phys. **70**, 1975–1979.
[14]D. Johnson, J. Koplik, and R. Dashen, "Theory of dynamic permeability and tortuosity in fluid-saturated porous media," J. Fluid Mech. **176**, 379–402 (1987).
[15]L. Botten, N. Nicorovici, A. Asatryan, R. McPhedran, C. Poulton, C. de Sterke, and P. Robinson, "Formulation for electromagnetic scattering and propagation through grating stacks of metallic and dielectric cylinders for photonic crystal calculations. Part I Method," J. Opt. Soc. Am. A **17**, 2165–2176 (2000).
[16]S. Wilcox, L. Botten, R. McPhedran, C. Poulton, and C. de Sterke, "Modeling of defect modes in photonic crystals using the fictitious source superposition method," Phys. Rev. E **71**, 056606 (2005).
[17]C. Zwicker and C. Kosten, *Sound Absorbing Materials* (Elsevier, Amsterdam, 1949), p. 1.
[18]P. Barber and S. Hill, "Light Scattering by Particles: Computation Methods," in *Advanced Series in Applied Physics 2* (World Scientific, London, 1990), Chap. 2, p. 30.
[19]V. Twersky, "On scattering of waves by the infinite grating of circular cylinders," IRE Trans. Antennas Propag. **10**, 737–765 (1962).
[20]C. Linton, "Schlomilch series that arise in diffraction theory and their efficient computation," J. Phys. A **39**, 3325–3339 (2006).
[21]R. Brown and R. Bolt, "The measurement of flow resistance of porous acoustic materials," J. Acoust. Soc. Am. **13**, 337–344 (1942).
[22]P. Leclaire, L. Kelders, W. Lauriks, N. Brown, M. Melon, and B. Castagnède, "Determination of the viscous and thermal characteristic lengths of plastic foams by ultrasonic measurements in helium and air," J. Appl. Phys. **80**, 2009–2012 (1996).
[23]Z. Fellah, F. Mitri, M. Fellah, E. Ogam, and C. Depollier, "Ultrasonic characterization of porous materials: Inverse problem," J. Sound Vib. **302**, 746–759 (2007).
[24]R. Porter and D. Evans, "Rayleigh-bloch surface waves along periofidc gratings and their connection with trapped modes in waveguides," J. Fluid Mech. **386**, 233–258 (1999).
[25]R. Craster, S. Guenneau, and S. Adams, "Mechanism for slow waves near cutoff frequencies in periodic waveguides," Phys. Rev. B **79**, 045129 (2009).
[26]T. Utsunomiya and R. Eatck Taylor, "Trapped modes around a row of circular cylinders in a channel," J. Fluid Mech. **386**, 259–279 (1999).
[27]C. Cutler, "Electromagnetic waves guided by corruguated sturctures," Technical Report MM No. 44-160-218, Bell Telephone Lab (1944).